Auroral Morphological Changes to the Formation of Auroral Spiral during the Late Substorm Recovery Phase: Polar UVI and Ground All-Sky Camera Observations

Motoharu Nowada[1], Yukinaga Miyashita[2], Noora Partamies[3], Alexander William Degeling[4], and Quanqi Shi[5]

[1]Shandong University at Weihai
[2]Korea Astronomy and Space Science Institute
[3]The University Centre in Svalbard, Birkeland Centre for Space Science, University of Bergen, Norway
[4]Shandong University
[5]Shandong University, Weihai

November 25, 2022

Abstract

Polar ultraviolet imager (UVI) and an all-sky camera at Longyearbyen contemporaneously detected an auroral vortex structure (so-called "auroral spiral"). Particularly, from space, the auroral spiral was observed as a "small spot" in the poleward region of the main auroral oval near midnight, which was formed while the substorm-associated auroral bulge was subsiding and several poleward-elongated auroral streak-like structures appeared during the late substorm recovery phase. To pursue the spiral source region in the magnetotail, we trace each UVI image along field lines to the magnetic equatorial plane of the nightside magnetosphere using an empirical magnetic field model. Interestingly, the magnetotail region corresponding to the auroral spiral covered a broad region from X_{gsm} ~ -40 to -70 $_{E}$ at Y_{gsm} ~ 8 to 12 R_E. The appearance of this auroral spiral may suggest that extensive areas of the magnetotail remain active even during the late substorm recovery phase.

Figure 1

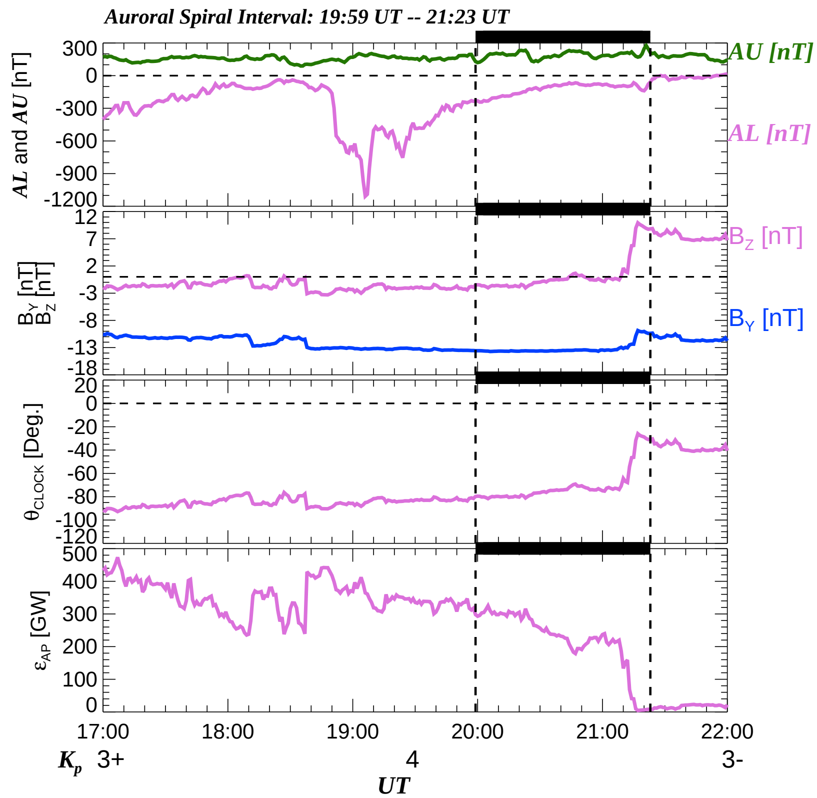

Auroral Spiral Interval: 19:59 UT -- 21:23 UT
AU [nT]
AL [nT]
AL and AU [nT]
300
0
-300
-600
-900
-1200
B_Z [nT]
B_Y [nT]
12
7
2
-3
-8
-13
-18
θ_{CLOCK} [Deg.]
20
0
-20
-40
-60
-80
-100
-120
ε_{AP} [GW]
500
400
300
200
100
0
17:00
18:00
19:00
20:00
21:00
22:00
K_p 3+
4
3-
UT

Figure 3

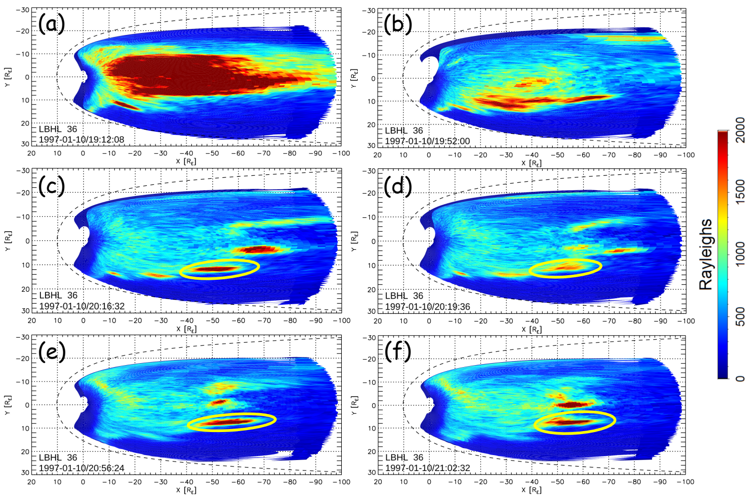
(a)
LBHL 36
1997-01-10/19:12:08
(b)
LBHL 36
1997-01-10/19:52:00
(c)
LBHL 36
1997-01-10/20:16:32
(d)
LBHL 36
1997-01-10/20:19:36
(e)
LBHL 36
1997-01-10/20:56:24
(f)
LBHL 36
1997-01-10/21:02:32
Y [R$_E$]
X [R$_E$]
Rayleighs
0
500
1000
1500
2000

Auroral Morphological Changes to the Formation of Auroral Spiral during the Late Substorm Recovery Phase: Polar UVI and Ground All-Sky Camera Observations

Motoharu Nowada[1†], Yukinaga Miyashita[2,3], Noora Partamies[4,5], Alexander William Degeling[1], and Quan-Qi Shi[1]

[1] Shandong Key Laboratory of Optical Astronomy and Solar-Terrestrial Environment, School of Space Science and Physics, Institute of Space Sciences, Shandong University, Weihai, Shandong, People's Republic of China.

[2] Korea Astronomy and Space Science Institute, Daejeon, South Korea.

[3] Korea University of Science and Technology, Daejeon, South Korea.

[4] Department of Arctic Geophysics, The University Centre in Svalbard, Norway.

[5] Birkeland Centre for Space Science, Norway.

[†]Corresponding author: Motoharu Nowada (moto.nowada@sdu.edu.cn)

Key Points:

- Auroral morphological changes prior to and during auroral spiral appearance in the late substorm recovery phase are investigated.
- The source region of the auroral spiral in the magnetotail is extensively distributed over 30 R_E, from X_{gsm} ~ -40 to -70 R_E.
- Extensive areas of the magnetotail are active enough to cause auroral spirals even during the late substorm recovery phase.

Running Title: Auroral Spiral in Late Substorm Recovery

Keyword: Auroral Spiral; Substorm; Late Recovery Phase of Substorm; Simultaneous Space- and Ground-based Observations

Abstract

Polar ultraviolet imager (UVI) and an all-sky camera at Longyearbyen contemporaneously detected an auroral vortex structure (so-called "auroral spiral"). Particularly, from space, the auroral spiral was observed as a "small spot" in the poleward region of the main auroral oval near midnight, which was formed while the substorm-associated auroral bulge was subsiding and several poleward-elongated auroral streak-like structures appeared during the late substorm recovery phase. To pursue the spiral source region in the magnetotail, we trace each UVI image along field lines to the magnetic equatorial plane of the nightside magnetosphere using an empirical magnetic field model. Interestingly, the magnetotail region corresponding to the auroral spiral covered a broad region from X_{gsm} ~ -40 to -70 R_E at Y_{gsm} ~ 8 to 12 R_E. The appearance of this auroral spiral may suggest that extensive areas of the magnetotail remain active even during the late substorm recovery phase.

Plain Language Summary

Auroras that are locally observed to possess a vortex structure are frequently referred to as auroral spirals. The fundamental features of auroral spirals, such as their generation process and source region in the magnetotail, are not well understood. Based on the images obtained from the Polar UVI instrument and an all-sky camera installed at Longyearbyen, we examined the morphological changes prior to and during an auroral spiral event which occurred as the nightside magnetosphere recovered after a substorm on 10 January 1997. The auroral spiral was formed while auroral features associated with the substorm subsided and followed several poleward-elongated auroral streak-like structures disappeared. The magnetotail source region of the auroral spiral spanned a broad region in the magnetotail, from 40 to 70 R_E in the anti-sunward direction with a dawn-dusk width of ~ 4 R_E. These estimates are made by projecting the UVI image of the auroral spiral in the ionosphere along field lines to the nightside magnetic equatorial plane using an empirical geomagnetic field model. These results suggest that extensive areas of the magnetotail are active enough to cause auroral spirals even during the late substorm recovery phase.

1. Introduction

Auroral phenomena with vortex structures (auroral spirals) have been frequently observed by ground-based all-sky cameras and polar-orbiting satellites. Their fundamental characteristics, such as their appearance locations and spiral diameters, have been discussed by Davis and Hallinan (1976), Partamies et al. (2001a, b), Voronkov et al. (2000), and references therein. Partamies et al. (2001a) and Davis and Hallinan (1976) independently obtained statistical distributions of auroral spirals in magnetic local time (MLT) and magnetic latitudes (MLat), based on all-sky camera observations. Most of the auroral spirals were distributed over the nightside ionosphere from 18 h to 5 h MLT, while their MLat distributions were concentrated around 65° (Partamies et al. 2001a), or between 70° and 80° (Davis and Hallinan, 1976), although there were constraints of field of view based on the all-sky camera locations. Depending on the study, the scale (diameter) of the auroral spiral varies between 25 and 75 km (Partamies et al. 2001a, 2001b), or between 20 and 1,300 km (Davis and Hallinan, 1976).

Keiling et al. (2009a, 2009b) examined an auroral spiral event which occurred during an auroral substorm, from the onset to the expansion phase; this event was associated with fast earthward plasma flows, an abrupt increase of the northward magnetic field (dipolarization), and energetic particle injections, based on in situ magnetotail observations. These authors obtained a series of images of auroral development from auroral breakup (onset of poleward expansion of the aurora) to auroral spiral decay using the THEMIS all-sky images. Because the spirals were observed during the substorm expansion phase, they were formed and decayed in conjunction with repetitive shrinking-and-stretching of multiple arcs associated with substorm growth, and in the westward travelling surges (e.g., Roux et al. 1991). The complete auroral spiral was short-lived (less than 10 s), and the time scale from formation to decay was ~ 1 min. The average diameter of the observed spirals was 200 – 300 km.

However, as pointed out by Partamies et al. (2001a), the occurrence probability of auroral spirals is higher at geomagnetically quiet times without substorm activity than during the substorm onset and expansion phases. The auroral morphological changes to the complete auroral spiral formation during the substorm recovery phase, particularly at its late stage, have not yet been reported and examined. Keiling et al. (2009a, 2009b) concluded that auroral spirals are produced by field-aligned currents (FACs) initiated by flow shears (vortices) between magnetotail reconnection-generated fast plasma flows and slower background plasma sheet flows. However, the auroral spirals exhibit not only substorm activity dependence but also relatively broad MLT and MLat distributions (Davis and Hallinan, 1976; Partamies et al. 2001a). Therefore, the source region in the magnetotail and/or formation mechanism of all auroral spirals are most likely not always the same.

In this letter, we examine the morphological changes of auroral spirals prior to and during the late substorm recovery phase and the associated variations of the auroral source region in the magnetotail, based on the Polar UVI observations. The instrumentation is described in Section 2. In Section 3, we show the solar wind conditions and the results of Polar UVI observation. The summary and discussions of this study are described in Section 4.

2. Instrumentation

The ultraviolet imager (UVI) instrument onboard the Polar spacecraft, launched on 24 February 1996, provides global auroral imaging data (Torr et al., 1995). The UVI images used in this study consist of long Lyman-Birge-Hopfield emission (LBHL; ~170 nm) and short LBH emission (LBHS; ~150 nm) images. The integration times of the Polar UVI data are 18 s and 36 s. In this study, the UVI images are displayed in altitude adjusted corrected geomagnetic (AACGM; Baker and Wing, 1989) and geographic coordinates.

The all-sky camera (ASC) installed at the Longyearbyen station (75.32° magnetic latitude and 111.0° magnetic longitude) covers a circular area with a diameter of about 600 km at 110 km altitude with a field of view (FOV) of 140°. Because the number of pixels corresponding to a 140° field of view is 440×440, the average spatial resolution is 1.36 km/pixel (600 km/440 pixels). The time resolution of the ASC's images filtered at 558 nm is 20 s for the time interval of interest.

3. Observations

Figure 1 shows the solar wind parameters and geomagnetic indices for 5 h between 17:00 UT and 22:00 UT. From top to bottom panels indicate the *AL* and *AU* indices, the GSM-Y and -Z components of the interplanetary magnetic field (IMF-B_y and -B_z), the IMF clock angle which was derived by arctan(IMF-B_y/IMF-B_z), and the Akasofu-Perreault parameter (ε_{AP}), which is a measure of the solar wind energy input rate (Perreault and Akasofu, 1978). The K_p index is also shown at the bottom of the figure. During this interval, the entire cycle of a substorm driving moderate geomagnetic disturbances with a K_p range from 3- to 4 can be found. *AL* shows a sharp, large decrease from ~18:45 UT (the substorm onset) to ~19:05 UT, and then *AL* recovered to ~ 0 nT at ~21:23 UT. The interval of the auroral spiral was identified by visual inspection, based on the data from Polar UVI and the all-sky camera (ASC) installed at the Longyearbyen station, and persisted from 19:59 UT to 21:23 UT (bracketed by two black broken lines with horizontal thick bars) during the late recovery phase of the substorm. Clear jumps were seen in the associated IMF-B_y and -B_z components at 21:10 UT. In particular, IMF-B_z turned from long-lived (at least 4 h) weak southward (negative) to northward (positive) directions, while IMF-B_y had a dominantly dawnward (negative) component. The clock angle became increased from -75° to -25° in association with this abrupt IMF-B_z jump. Accordingly, the ε parameter shows a significant decrease associated with the jumps of the IMF and clock angle, which was preceded by a gradual decrease during the first half of the spiral interval. Note that the increasing trend of the ε parameter before the spiral from ~18:10 UT to ~19:15 UT may have caused the substorm.

Corresponding auroral activity and its morphological changes under these solar wind conditions are shown in Figure 2. A series of the representative auroral images before the onset of the spiral is shown in Figures 2a and 2b, which correspond to the early and late substorm recovery phases, respectively. The substorm-associated auroral bulge azimuthally extended from 23 h to 4 h MLT along the main auroral oval (Figure 2a), and reduced in size and intensity with time. Several poleward-elongated auroral streak-like structures were found to remain in place as the auroral bulge subsided (Figure 2b). As seen in Figure 2c, the auroras changed their forms from several elongated streak-like structures to four azimuthally-lined small spots, which are seen from 20 h to 1 h MLT. The spot at ~ 23 h MLT, highlighted with a yellow oval, corresponds to the aurora with significant vortex structure, that is, the auroral spiral seen at Longyearbyen. Such azimuthally-lined auroral spots in the poleward region of the main auroral oval from the pre-midnight to midnight sectors have been detected previously with the Viking UV imager, but were not discussed in detail, because they were identified as the poleward component of "double auroral oval" (Elphinstone et al. 1995). The simultaneous all-sky camera (ASC) images at Longyearbyen are shown in Figures 2g and 2h, in which the auroral spiral is clearly visible in the southern part of the ASC's FOV. The rotational sense of the observed spiral is anti-clockwise, when viewed from the direction of the magnetic field. From the ASC's images in geographical coordinates (see Figure S3), we roughly estimated the scales (diameters) of the auroral spirals with various directional patterns, and summarized their average scales in Table 1. Here, we estimated the two kinds of spiral scale for each time using 1° in geographical latitude = 111 km: the core part (central part of intense aurora) and the core part with the spiral arms. The actual calculations were performed using Latitude/Longitude Distance Calculator, which was developed by National Hurricane Center and Central Pacific Hurricane Center (https://www.nhc.noaa.gov/gccalc.shtml), by giving the geographical latitudes and longitudes at the two different edge points of the spiral.

As the substorm recovery proceeded, several intense spots were clearly seen in the poleward region of the main auroral oval (Figures 2d and 2e). Figures 2i and 2j show the ASC's images from the Longyearbyen station for the times nearest to the Polar UVI observation times (20:56:20 UT and 21:02:20 UT). The FOV of the ASC is highlighted with a yellow oval in Figures 2d and 2e. Auroral spirals clearer than the previous spirals (Figures 2g and 2h) can be found. They moved southwestward with anti-clockwise rotation, compared with the previous spirals (more clearly seen in Figure S3 and Movie S1). The average scale (diameter) of the core part (core + arm part) of the detected spiral was about 150 – 180 km (260 – 320 km). To check whether or not the auroral spot detected by the Polar UVI corresponds to the spiral observed by the Longyearbyen ASC, we compared the plots of the UVI data in geographical coordinates (Figure 2f) with the spiral images observed at Longyearbyen (Figures 2g, 2h, 2i and 2j). The auroral spiral (yellow oval) detected by Polar covers the southern region of Longyearbyen on Svalbard island, demonstrating that the auroral spiral seen by the Polar UVI is identical with that detected by the ASC at Longyearbyen. Also looking at Figure S3, the geographical latitudes and longitudes of the spiral from Longyearbyen were consistent with those of the Polar observations.

Although the auroral morphological changes to the spiral are clarified, we do not have any observations of the source region of the spiral and its temporal and spatial variations. To pursue the source region of the auroral spiral and its variations, we made magnetic equatorial plane projection maps, where each pixel of the Polar UVI images was traced to the GSM X-Y plane of the magnetotail along the magnetic field line, based on an empirical magnetic field model – Tsyganenko 96 model (Tsyganenko and Stern, 1996). In this mapping, however, we removed the limitation of the maximum trace distance which was set in the model: radius of a sphere, defining the outer boundary of the tracing. Figure 3 shows the projection maps of the UVI images onto the GSM X-Y plain for the times of the auroral bulge (Figure 3a), poleward-elongated streak-like structures (Figure 3b), and auroral spirals (Figures 3c to 3f). These times are the same as those of Figure 2f. Such mappings to the magnetic equator have already been established and implemented by many researchers (e.g., Elphinstone et al. 1993; Lu et al. 1999, 2000; Pulkkinen et al. 1995, 1998; and references therein). Note that these mapping results of the auroras onto equatorial X-Y locations may sensitively depend on magnetic field models used, as suggested by Lu et al. (2000; see their Plate 3).

In Figures 3a and 3b, the projection maps before the spiral formation are shown. The auroral bulge azimuthally extended in the ionosphere is broadly projected onto the magnetotail. The particularly intensified part (dark red part) extends from X_{gsm} ~ -10 to -90 R_E and Y_{gsm} ~ -10 to 10 R_E. The auroral elongated streak-like structures are also distributed from X_{gsm} ~ -20 to -40 R_E or, at most, -70 R_E in the duskside (Figure 3b). The auroral spiral detected by the ASC at Longyearbyen (Figures 3c to 3f) broadly covers the magnetotail region from X_{gsm} ~ -40 to -70 R_E at Y_{gsm} ~ 8 to 12 R_E, as highlighted with a yellow oval. The projected auroral elongated streak-like structures are “elliptically” distributed from the duskside to the dawnside of the magnetotail.

4. Summary and Discussions

We examined the auroral morphological changes prior to and during auroral spiral appearances in the late substorm recovery phase, and found that the source region of the spirals extends over 30 R_E from -40 to -70 R_E downtail with a Y_{GSM} width of ~4 R_E according to mappings along field lines to the magnetotail. The substorm-associated bulge, which was azimuthally extended, became smaller as the substorm recovery proceeded, and the auroral morphology changed to several poleward-elongated streak-like structures. After these auroral streak-like structures, Polar detected that several small auroral spots were consecutively and azimuthally distributed in the poleward region of the main auroral oval near midnight. At least one of these spots was an auroral spiral as detected by the Longyearbyen ASC. Elphinstone et al. (1995) reported an observational case of azimuthally-lined small auroral spots at the poleward edge of the main auroral oval from pre-midnight to midnight. However, these spots occurred during the very early stage of the substorm recovery; the associated *AL* still kept its value of ~ -340 nT, and the intense substorm-associated auroral bulge structure still remained in the main auroral oval. These observations suggest that the spots of Elphinstone et al. (1995), which were potentially spirals, may be different from our case in the background environment of the auroral spiral formation.

Keiling et al. (2009a) also observed an auroral spiral, but their case was associated with auroral arc development and a westward traveling surge during the substorm expansion phase, unlike our auroral spiral during the late substorm recovery phase. Furthermore, the duration of our auroral spiral is different from that of Keiling's spiral case. Murphree and Elphinstone (1988) and Keiling et al. (2009a) pointed out that short-lived (less than 1 min) auroral spirals are expected to occur frequently during the (early and late) substorm recovery phases, and auroral spirals are one of the representative short-lived auroral phenomena. However, although the ASC at Longyearbyen detected repetitive formations and decays of auroral spirals, a single spiral with a duration much longer than the previous cases was also clearly seen (see Movie S1). Therefore, this observed spiral might differ from the short-lived auroral spiral during the substorm expansion phase that Keiling et al. (2009a) reported.

The detailed relationship between the spiral occurrence and the IMF orientation/variation still remains an open question. Although the IMF-B_z component changed its polarity from weakly negative to positive in the latter half of the spiral interval, no significant changes can be found in the spiral profile. The IMF clock angle was almost constant ($\theta_{CLOCK} \sim -95°$) prior to and during the spiral, suggesting that our auroral spiral might have occurred under weak but persistent large-scale plasma convection. The relationship between magnetic reconnection (rate) maintaining large-scale plasma convection and fundamental formation process of the spiral remains unclear. Elphinstone et al. (1995) and Murphree and Elphinstone (1998) discussed auroral spiral cases under northward IMF-B_z or IMF-$B_z \sim 0$ nT. Considering only the IMF conditions, our auroral spiral should be different from their cases. Partamies et al. (2001b) suggested that the winding of the auroral spiral can be attributed to local plasma processes, such as FAC enhancements. There are several essential problems to be elucidated, in particular: i) by what plasma phenomena in the magnetotail are auroral spirals basically formed; ii) why do they have locational and substorm phase dependences; and iii) how do spiral formation processes differ, depending on locations and substorm phases.

In this study, we first detected the auroral spots (spirals) during the late substorm recovery phase. Projecting the auroral spiral along field lines onto the magnetic equatorial plane of the magnetotail using an empirical geomagnetic field model, the spiral source region was extensively distributed from -40 to -70 R_E downtail. This result suggests that extensive areas of the magnetotail are active enough to cause auroral spirals even during the late substorm recovery phase.

Acknowledgments

M.N. enjoyed fruitful and constructive discussions with Jong-Sun Park and An-Min Tian, and was supported by a grant of the National Natural Science Foundation of China (NSFC 42074194). Y.M. was supported by Korea Astronomy and Space Science Institute under the R&D program (2022-1-850-09) supervised by the Ministry of Science and ICT. N.P. was supported by the Norwegian Research Council (NRC) under CoE contract 223252. Q.Q.S. was supported by NSFC 41731068, 41961130382, and 41974189, and also supported from International Space Science Institute, Beijing (ISSI-BJ). We thank George K. Parks for providing the Polar UVI data and Kan Liou for processing the data.

Data Accessibility

Polar ultraviolet imager (UVI) data can be accessed from https://cdaweb.gsfc.nasa.gov/pub/data/polar/uvi/uvi_level1/. Magnetometers – Ionospheric Radars – All-sky Cameras Large Experiment (MIRACLE) ASC quick-look data are available at https://space.fmi.fi/MIRACLE/ASC/, and ASC full resolution images and their numerical data used in this study can be downloaded from https://doi.org/10.5281/zenodo.6552492. The solar wind magnetic field and plasma OMNI data can be acquired from Coordinated Data Analysis Web (https://cdaweb.gsfc.nasa.gov/cdaweb/istp_public/), which is administrated by GSFC/NASA. We also thank the Helmholtz Centre Potsdam - GFZ German Research Centre for Geosciences and World Data Center for Geomagnetism, Kyoto for accessing the data of the K_p, AU, and AL indices from https://www.gfz-potsdam.de/en/kp-index and http://wdc.kugi.kyoto-u.ac.jp/index.html.

References

Baker, K. B., and Wing, S. (1989), A new magnetic coordinate system for conjugate studies at high latitudes, J. Geophys. Res. -Space Physics-, 94(A7), 9139– 9143, doi:10.1029/JA094iA07p09139.

Davis, T. N., and Hallinan, T. J. (1976), Auroral spirals, 1., Observations, J. Geophys. Res., 81, 3953 -3958, 1976.

Elphinstone, R. D., Murphree, J. S., Hearn, D. J., Heikkila, W., Henderson, M. G., Cogger, L. L., and Sandahl. I. (1993), The auroral distribution and its mapping according to substorm phase, J.

Atmos. Terr. Phys., 55, 1741.
Elphinstone, R. D., et al. (1995), The double oval UV auroral distribution: 1. Implications for the mapping of auroral arcs, J. Geophys. Res. -Space Physics-, 100(A7), 12075– 12092, doi:10.1029/95JA00326.
Keiling, A., Angelopoulos, V., Weygand, J. M., Amm, O., Spanswick, E., Donovan, E., Mende, S., McFadden, J., Larson, D., Glassmeier, K.-H., and Auster, H. U. (2009a), THEMIS ground-space observations during the development of auroral spirals, Ann. Geophys., 27, 4317 – 4332, https://doi.org/10.5194/angeo-27-4317-2009.
Keiling, A., et al. (2009b), Substorm current wedge driven by plasma flow vortices: THEMIS observations, J. Geophys. Res. - Space Physics -, 114, A00C22, doi:10.1029/2009JA014114.
Lu, G., Tsyganenko, N. A., Lui, A. T. Y., Singer, H. J., Nagai, T., and Kokubun, S. (1999), Modeling of time-evolving magnetic fields during substorms, J. Geophys. Res. -Space Physics-, 104(A6), 12327 – 12337, doi:10.1029/1999JA900145.
Lu, G., Brittnacher, M., Parks, G., and Lummerzheim, D. (2000), On the magnetospheric source regions of substorm-related field-aligned currents and auroral precipitation, J. Geophys. Res. -Space Physics-, 105(A8), 18483 – 18493, doi:10.1029/1999JA000365.
Murphree, J. S., and Elphinstone, R. D. (1988), Correlative studies using the Viking imagery, Adv. Space Res. 8(9 – 10), pp. (9)9 – (9)19.
Partamies, N., Kauristie, K., Pulkkinen, T. I., and Brittnacher, M. (2001a), Statistical study of auroral spirals, J. Geophys. Res. -Space Physics-, 106(A8), 15415 – 15428, doi:10.1029/2000JA900172.
Partamies, N., Freeman, M. P., and Kauristie, K. (2001b), On the winding of auroral spirals: Interhemispheric observations and Hallinan’s theory revisited, J. Geophys. Res. -Space Physics-, 106(A12), 28913 – 28924, doi:10.1029/2001JA900093.
Perreault, P., and Akasofu, S. -I. (1978), Study of geomagnetic storms, Geophys. J. R. Astron. Soc., 54, 547.
Pulkkinen, T. I., Baker, D. N., Pellinen, R. J., Murphree, J. S., and Frank, L. A. (1995), Mapping of the auroral oval and individual arcs during substorms, J. Geophys. Res. -Space Physics-, 100(A11), 21987 – 21994, doi:10.1029/95JA01632.
Pulkkinen, T. I., et al. (1998), Two substorm intensifications compared: Onset, expansion, and global consequences, J. Geophys. Res. -Space Physics-, 103(A1), 15 – 27,

doi:10.1029/97JA01985.

Roux, A., Perraut, S., Robert, P., Morane, A., Pedersen, A., Korth, A., Kremser, G., Aparicio, B., Rodgers, D., and Pellinen, R. (1991), Plasma sheet instability related to the westward traveling surge, J. Geophys. Res. -Space Physics-, 96(A10), 17697 – 17714, doi:10.1029/91JA01106.

Torr, M. R., Torr, D. G., Zukic, M., Johnson, R. B., Ajello, J., Banks, P., Clark, K., Cole, K., Keffer, C., Parks, G., Tsurutani, B., and Spann, J. (1995), A far ultraviolet imager for the International Solar-Terrestrial Physics Mission, Space Science Reviews 71 (1-4), 329 – 383.

Tsyganenko, N. A., and Stern, D. P. (1996), Modeling the global magnetic field of the large-scale Birkeland current systems. Journal of Geophysical Research -Space Physics-, 101(A12), 27187 – 27198, https://doi.org/10.1029/96JA02735.

Voronkov, I., Donovan, E. F., Jackel, B. J., and Samson, J. C. (2000), Large-scale vortex dynamics in the evening and midnight auroral zone: Observations and simulations, J. Geophys. Res. -Space Physics-, 105(A8), 18505– 18518, doi:10.1029/1999JA000442.

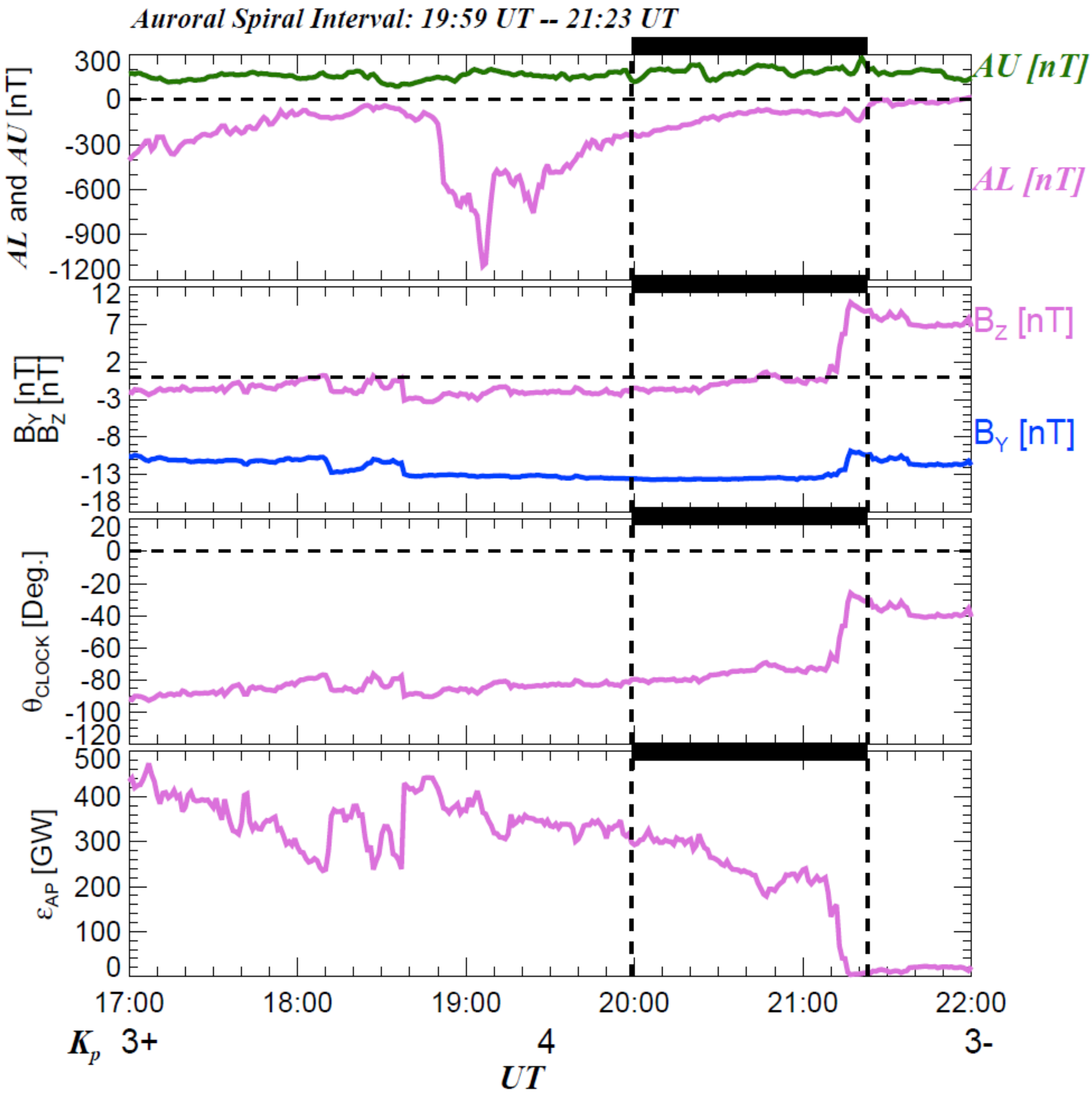

Figure 1. Plots of solar wind parameters and geomagnetic activity indices during 5 h from 17:00 UT to 22:00 UT are shown. From top to bottom panels display the *AL* and *AU* indices, the IMF-B_y and -B_z components, the IMF clock angle (arctan(IMF-B_y/IMF-B_z)), and the Akasofu-Pelleaut parameter (ε_{AP}), obtained with $V_{SW}B_t^2\sin^4(\theta_{CLOCK}/2)(4\pi L_0^2/\mu_0)$, where V_{SW} is the solar wind velocity, B_t = sqrt(IMF-B_x^2 + IMF-B_y^2 + IMF-B_z^2), and L_0 = 7.0 R_E. The K_p index is indicated at the bottom of the figure. The auroral spiral interval from 19:59 UT to 21:23 UT is indicated with horizontal thick bars and also bracketed with black broken vertical lines.

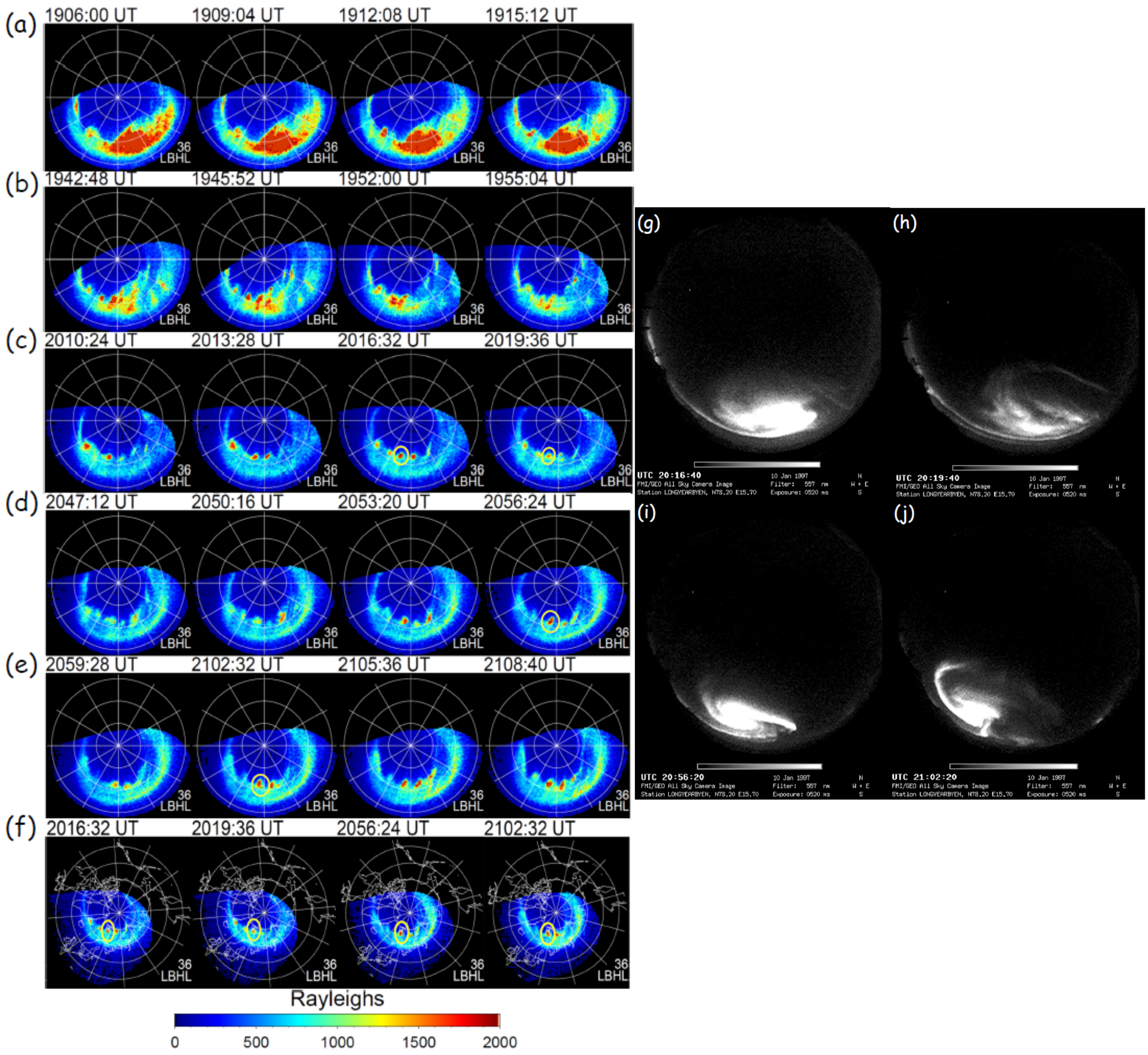

Figure 2. Consecutive Lyman-Birge-Hopfield long (LBHL) emission snapshots taken from the Polar ultraviolet imager (UVI) in altitude adjusted corrected geomagnetic (AACGM) coordinates (Baker and Wing, 1989) prior to (panels a and b) and during (panels c, d, and e) the auroral spiral are shown. The integration time of each image is 36.8 s. In panel f, four snapshots of LBHL-36s images for the nearest auroral spiral times, identified with the all-sky camera (ASC) images from Longyearbyen, are shown in geographic coordinates. Each panel is oriented such that the bottom, right, top, and left correspond to midnight (24 h magnetic local time; MLT), dawn (6 h MLT), noon (12 h MLT), and dusk (18 h MLT), respectively. The white circles are drawn every 10° from

60° to 80° magnetic latitude (MLat) for panels a – e and from 50° to 80° for panel f. The white lines are drawn every 2 h in MLT. The color code is assigned according to the auroral brightness in units of Rayleigh. Panels g, h, i, and j show the images of the auroral spiral taken from the ASC installed at Longyearbyen. The approximate field of view of the ASC is marked with yellow circles in the UVI plots in panels c, d, e, and f.

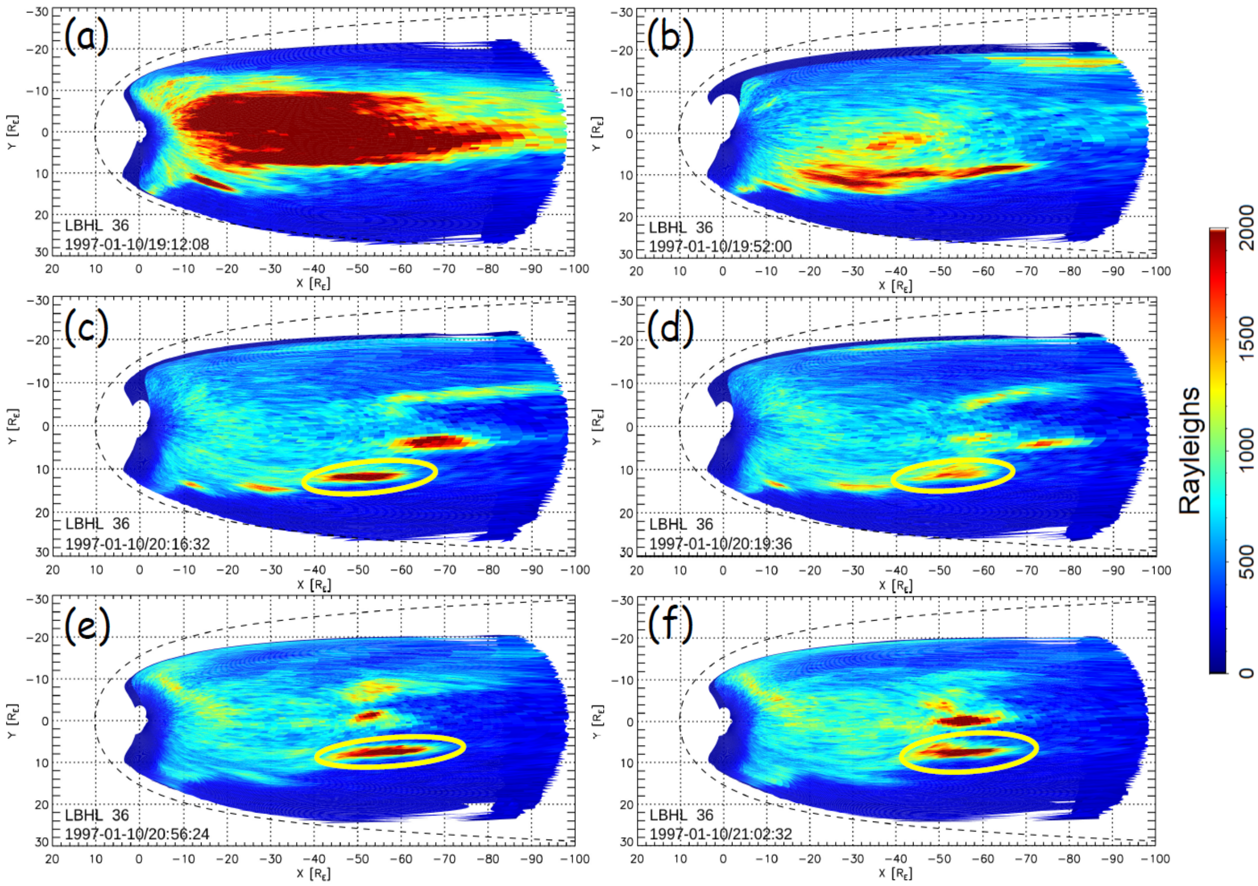

Figure 3. Magnetic equatorial projection maps of Polar UVI auroral pixel data prior to (panels a and b) and during (panels c, d, e, and f) the auroral spiral are shown. Each pixel was traced to the GSM X-Y plane of the magnetotail, based on the Tsyganenko 96 geomagnetic field model (Tsyganenko and Stern, 1996). Yellow ovals indicate the auroral spirals detected by the Polar UVI and the ASC at Longyearbyen. The color code shows the auroral brightness in units of Rayleigh. The dotted curve indicates the model magnetopause location derived from Shue et al. (1998).

Table 1. Rough scales (diameters) of the spiral core part (central part of intense auroral brightness) and the core part with the spiral arms are summarized. These scales are estimated from the ASC's images in geographical coordinates using 1° in geographical latitude = 111 km and the distance (km) corresponding to the geographical longitude where the auroral spiral was observed for each time. The calculations were performed with Latitude/Longitude Distance Calculator, developed by National Hurricane Center and Central Pacific Hurricane Center (https://www.nhc.noaa.gov/gccalc.shtml), by giving the geographical latitudes and longitudes at the two different edge points of the spiral.

Time [UT]	Average scale of core part [km]	Average scale of core part + spiral arms [km]
20:16:40	250	350
20:19:40	130	300
20:56:20	180	260
21:02:20	150	320

Geophysical Research Letters

Supporting Information for

Auroral Morphological Changes to the Formation of Auroral Spiral during the Late Substorm Recovery Phase: Polar UVI and Ground All-Sky Observations

Motoharu Nowada[1†], Yukinaga Miyashita[2,3], Noora Partamies[4,5], Alexander William Degeling[1], and Quan-Qi Shi[1]

[1] Shandong Key Laboratory of Optical Astronomy and Solar-Terrestrial Environment, School of Space Science and Physics, Institute of Space Sciences, Shandong University, Weihai, Shandong, People's Republic of China.

[2] Korea Astronomy and Space Science Institute, Daejeon, South Korea.

[3] Korea University of Science and Technology, Daejeon, South Korea.

[4] Department of Arctic Geophysics, The University Centre in Svalbard, Norway.

[5] Birkeland Centre for Space Science, Norway.

Contents of this file

Introduction

Time-series of Polar ultraviolet imager (UVI) data of Lyman-Birge-Hopfield long (LBHL) emission with an integration time of 36.8 s is shown to examine the global auroral morphological changes before and during the formation of the aurora spiral from 19:59 UT to 21:23 UT on January 10, 1997. The UVI data are shown in two different coordinates: altitude adjusted corrected geomagnetic (AACGM) (Figure S1) and geographic coordinates (Figure S2) from 18:41:28 UT to 21:57:44 UT. The all-sky camera (ASC) images in geographic coordinates are also shown to help discuss the spiral position and motion relative to the ASC's field of view (Figure S3). All UVI data were obtained from the Northern Hemisphere. Here, we also show a movie of consecutive images obtained from ASC installed at the Longyearbyen station for 2 h from 20:00 UT to 22:00 UT, when the auroral spiral interval is covered (Movie S1).

Figure S1

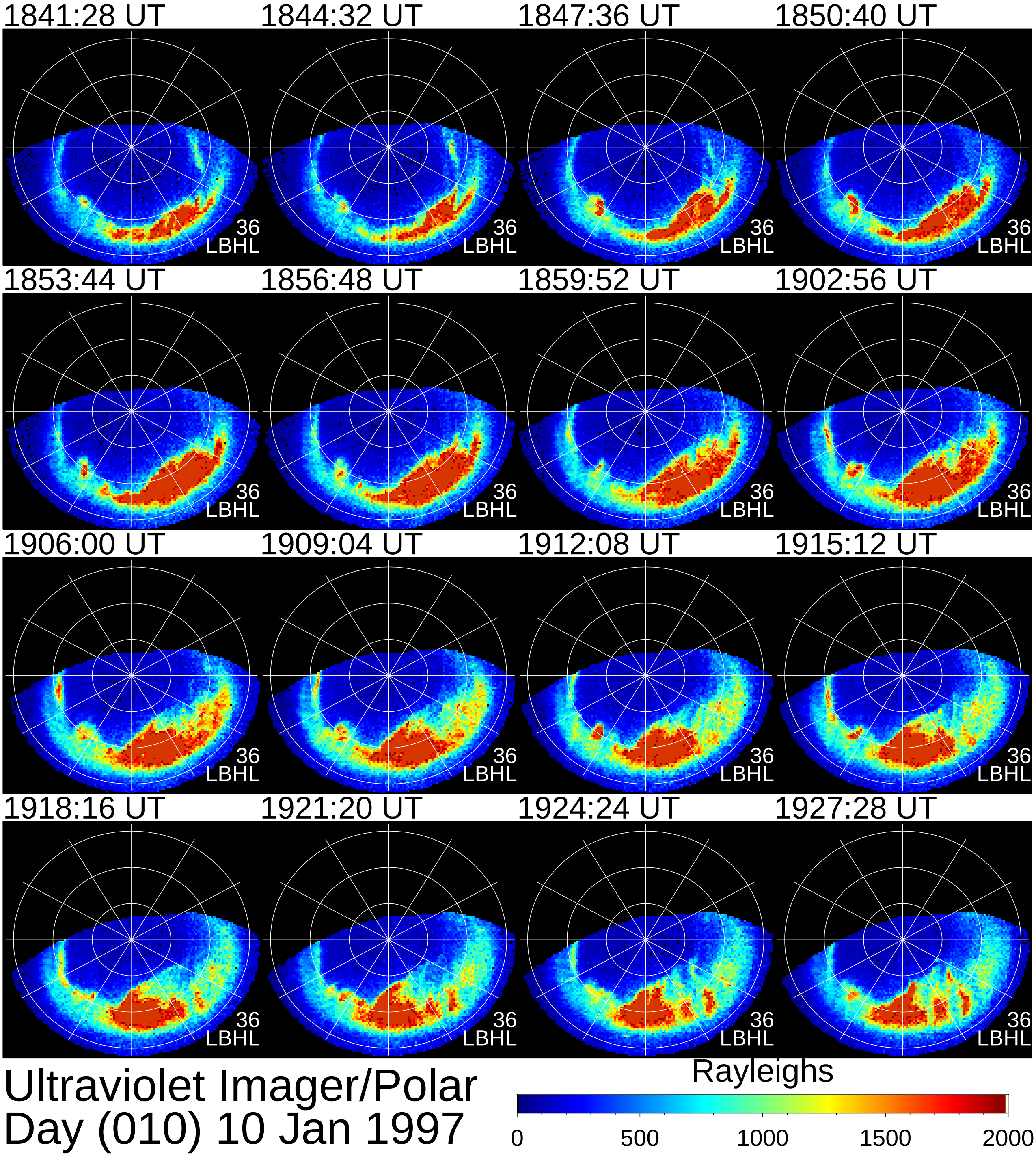
1841:28 UT
1844:32 UT
1847:36 UT
1850:40 UT
1853:44 UT
1856:48 UT
1859:52 UT
1902:56 UT
1906:00 UT
1909:04 UT
1912:08 UT
1915:12 UT
1918:16 UT
1921:20 UT
1924:24 UT
1927:28 UT
36
LBHL
Ultraviolet Imager/Polar
Day (010) 10 Jan 1997
Rayleighs
0
500
1000
1500
2000

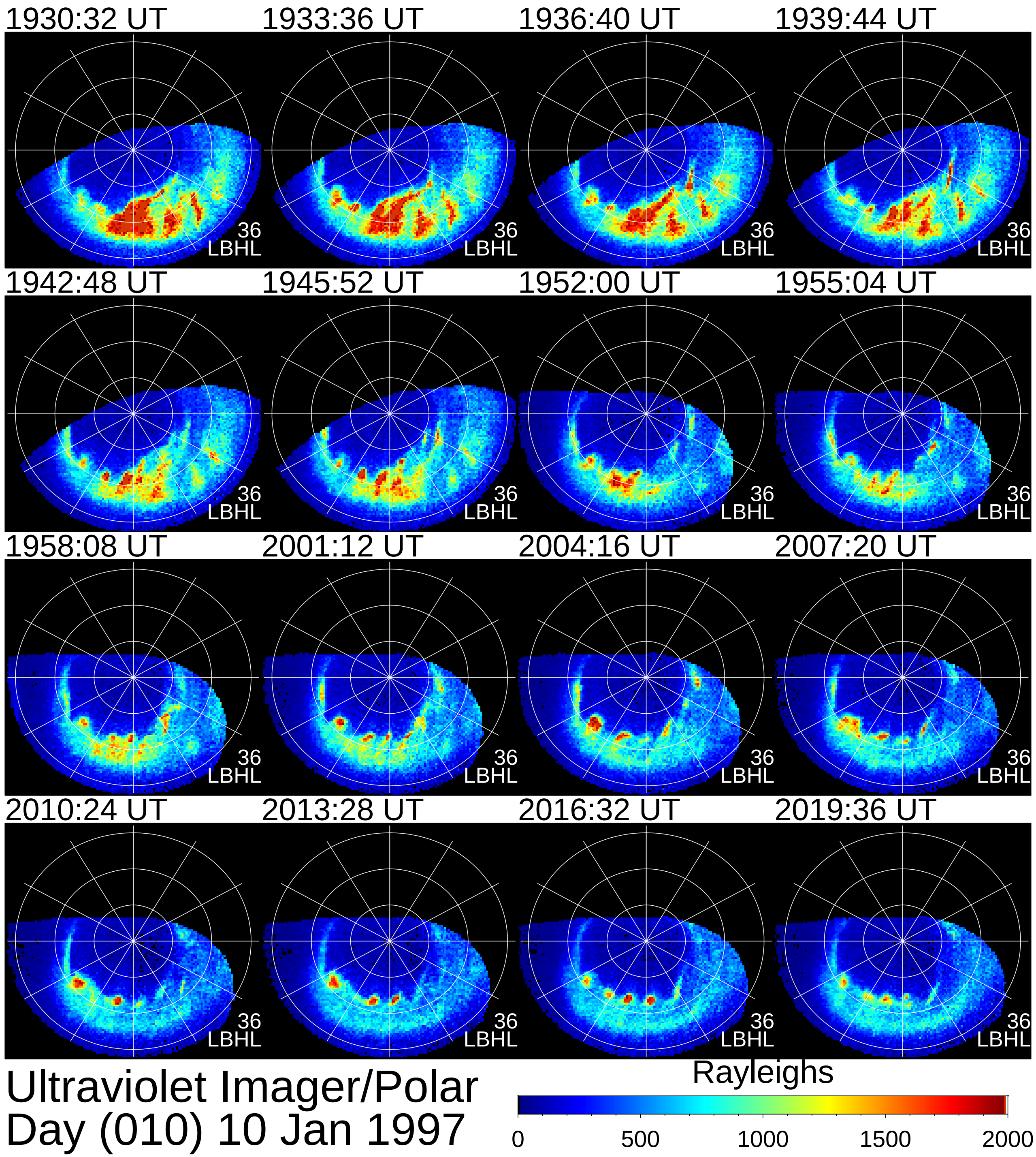
1930:32 UT
1933:36 UT
1936:40 UT
1939:44 UT
1942:48 UT
1945:52 UT
1952:00 UT
1955:04 UT
1958:08 UT
2001:12 UT
2004:16 UT
2007:20 UT
2010:24 UT
2013:28 UT
2016:32 UT
2019:36 UT
36
LBHL
Ultraviolet Imager/Polar
Day (010) 10 Jan 1997
Rayleighs
0
500
1000
1500
2000

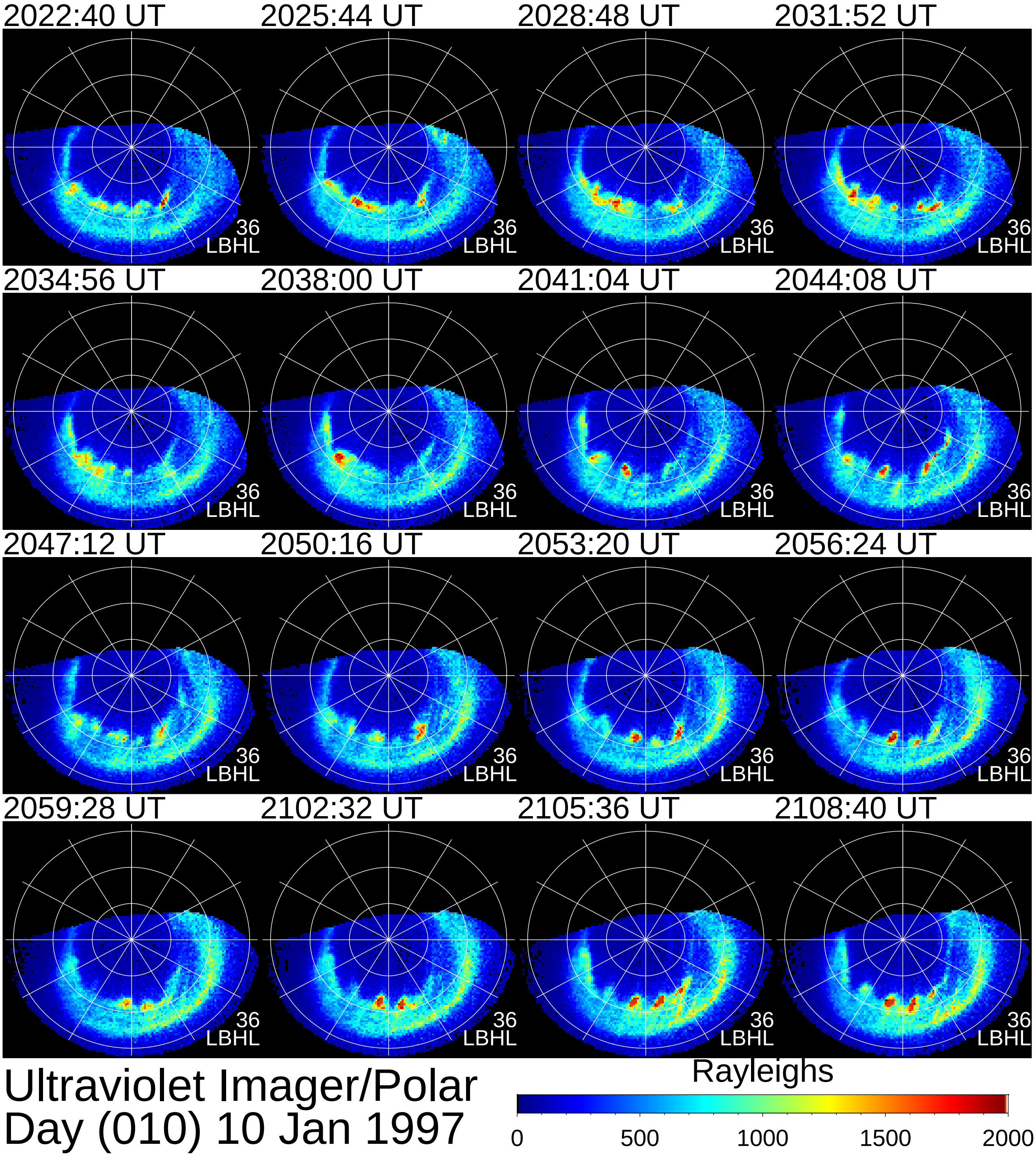
2022:40 UT
2025:44 UT
2028:48 UT
2031:52 UT
2034:56 UT
2038:00 UT
2041:04 UT
2044:08 UT
2047:12 UT
2050:16 UT
2053:20 UT
2056:24 UT
2059:28 UT
2102:32 UT
2105:36 UT
2108:40 UT
36
LBHL
Ultraviolet Imager/Polar
Day (010) 10 Jan 1997
Rayleighs
0
500
1000
1500
2000

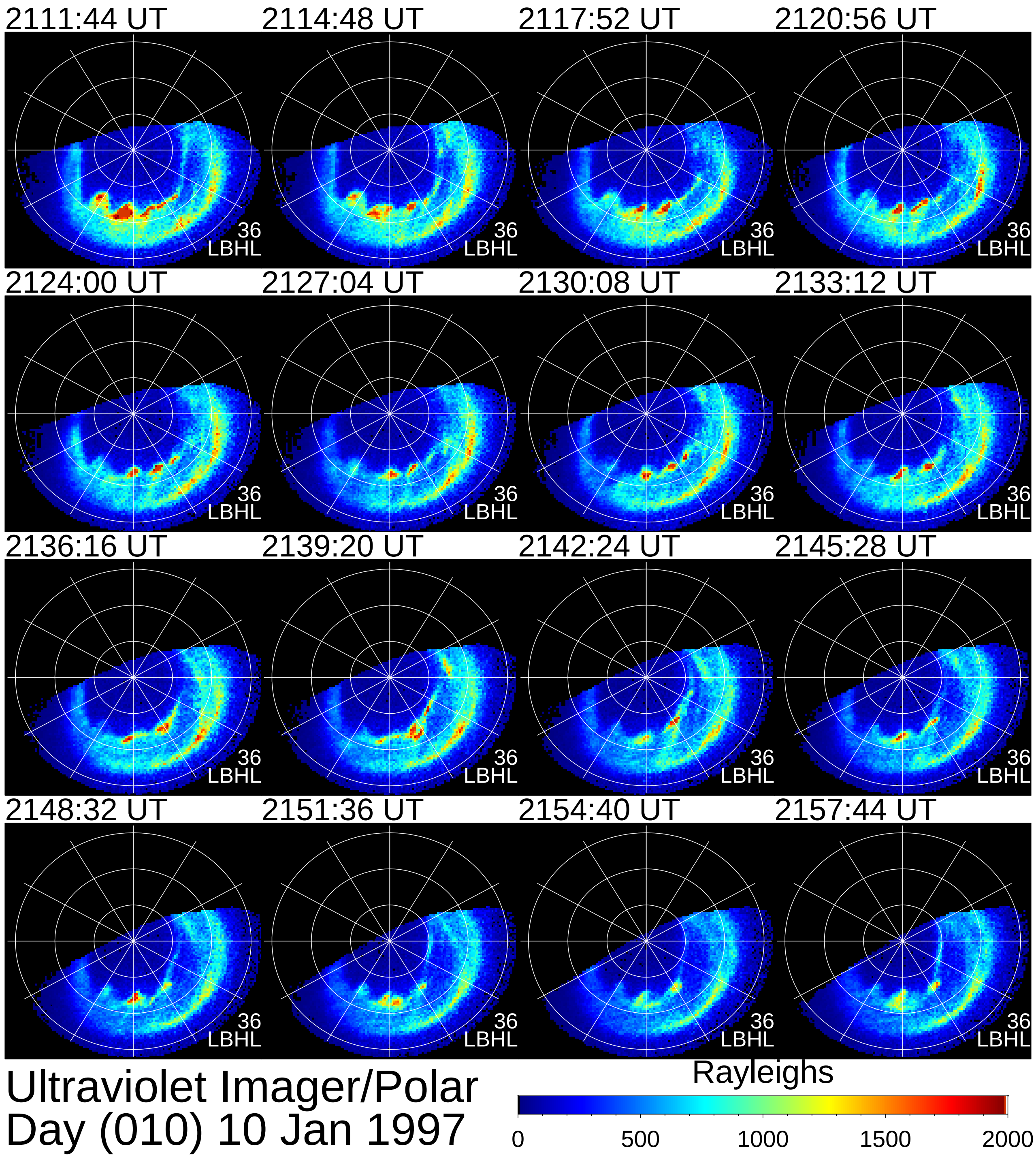

2111:44 UT
2114:48 UT
2117:52 UT
2120:56 UT
2124:00 UT
2127:04 UT
2130:08 UT
2133:12 UT
2136:16 UT
2139:20 UT
2142:24 UT
2145:28 UT
2148:32 UT
2151:36 UT
2154:40 UT
2157:44 UT
36
LBHL
Ultraviolet Imager/Polar
Day (010) 10 Jan 1997
Rayleighs
0
500
1000
1500
2000

Figure S2

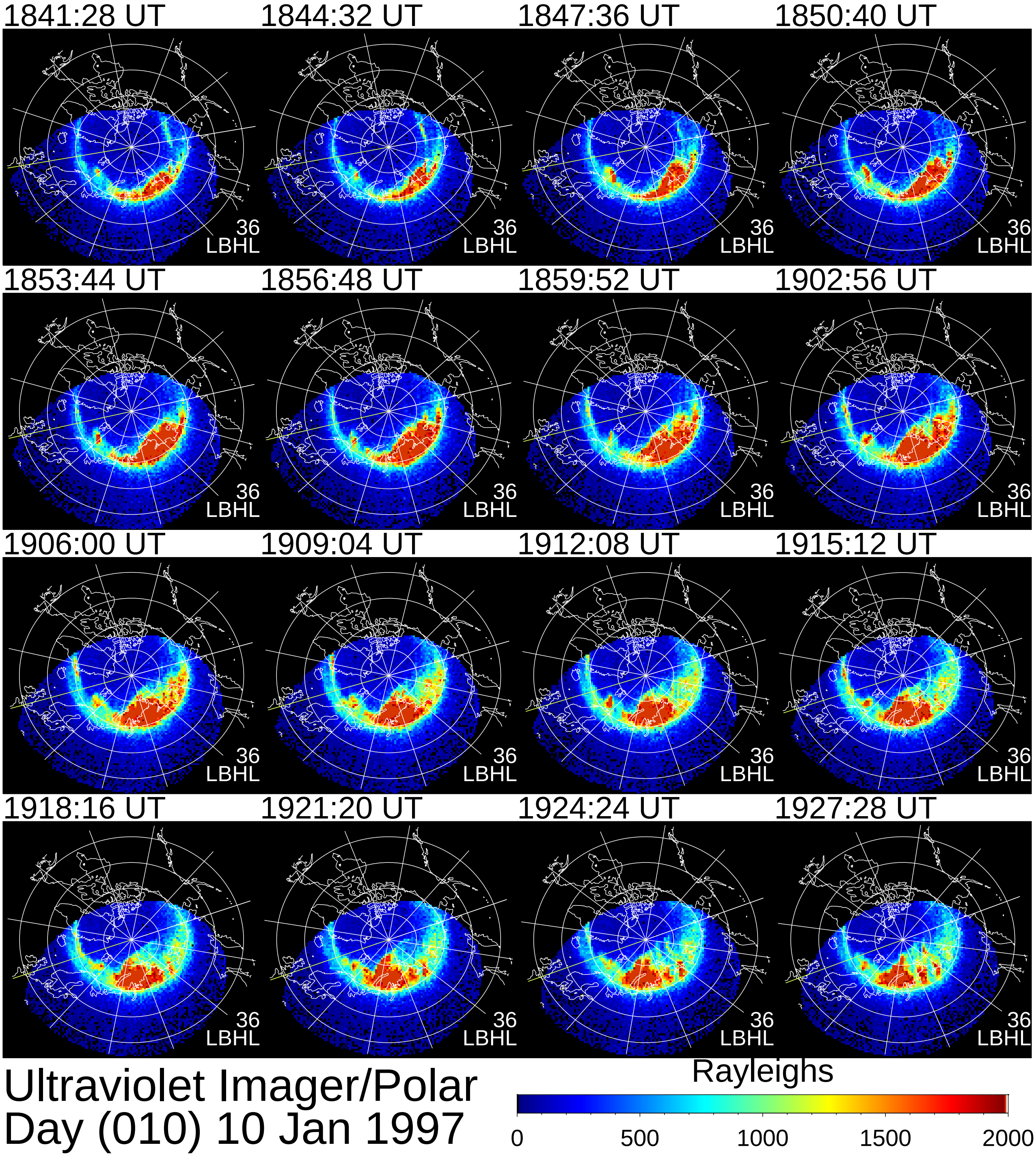
1841:28 UT
1844:32 UT
1847:36 UT
1850:40 UT
1853:44 UT
1856:48 UT
1859:52 UT
1902:56 UT
1906:00 UT
1909:04 UT
1912:08 UT
1915:12 UT
1918:16 UT
1921:20 UT
1924:24 UT
1927:28 UT
36
LBHL
Ultraviolet Imager/Polar
Day (010) 10 Jan 1997
Rayleighs
0
500
1000
1500
2000

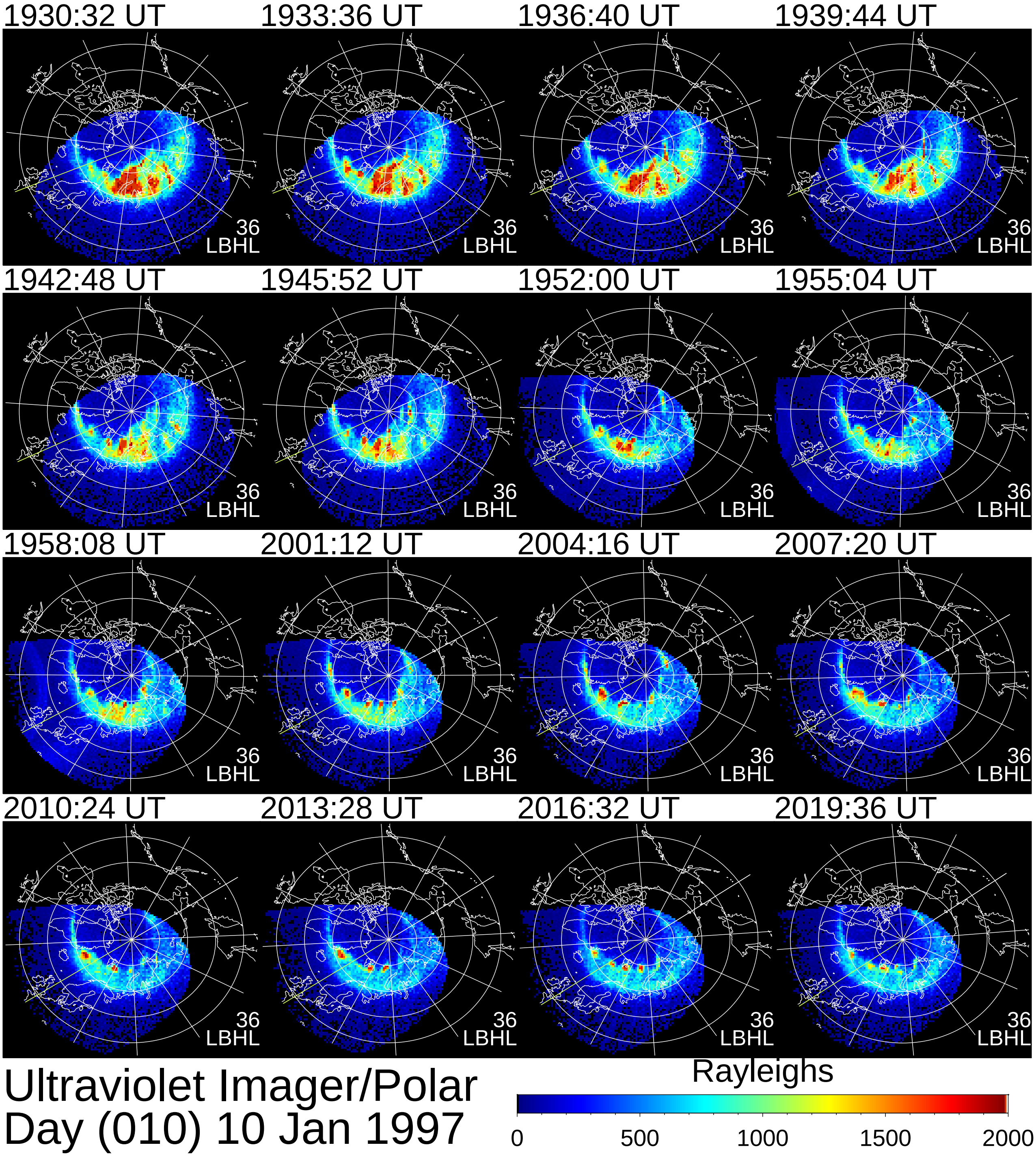
1930:32 UT
1933:36 UT
1936:40 UT
1939:44 UT
1942:48 UT
1945:52 UT
1952:00 UT
1955:04 UT
1958:08 UT
2001:12 UT
2004:16 UT
2007:20 UT
2010:24 UT
2013:28 UT
2016:32 UT
2019:36 UT
36
LBHL
Ultraviolet Imager/Polar
Day (010) 10 Jan 1997
Rayleighs
0
500
1000
1500
2000

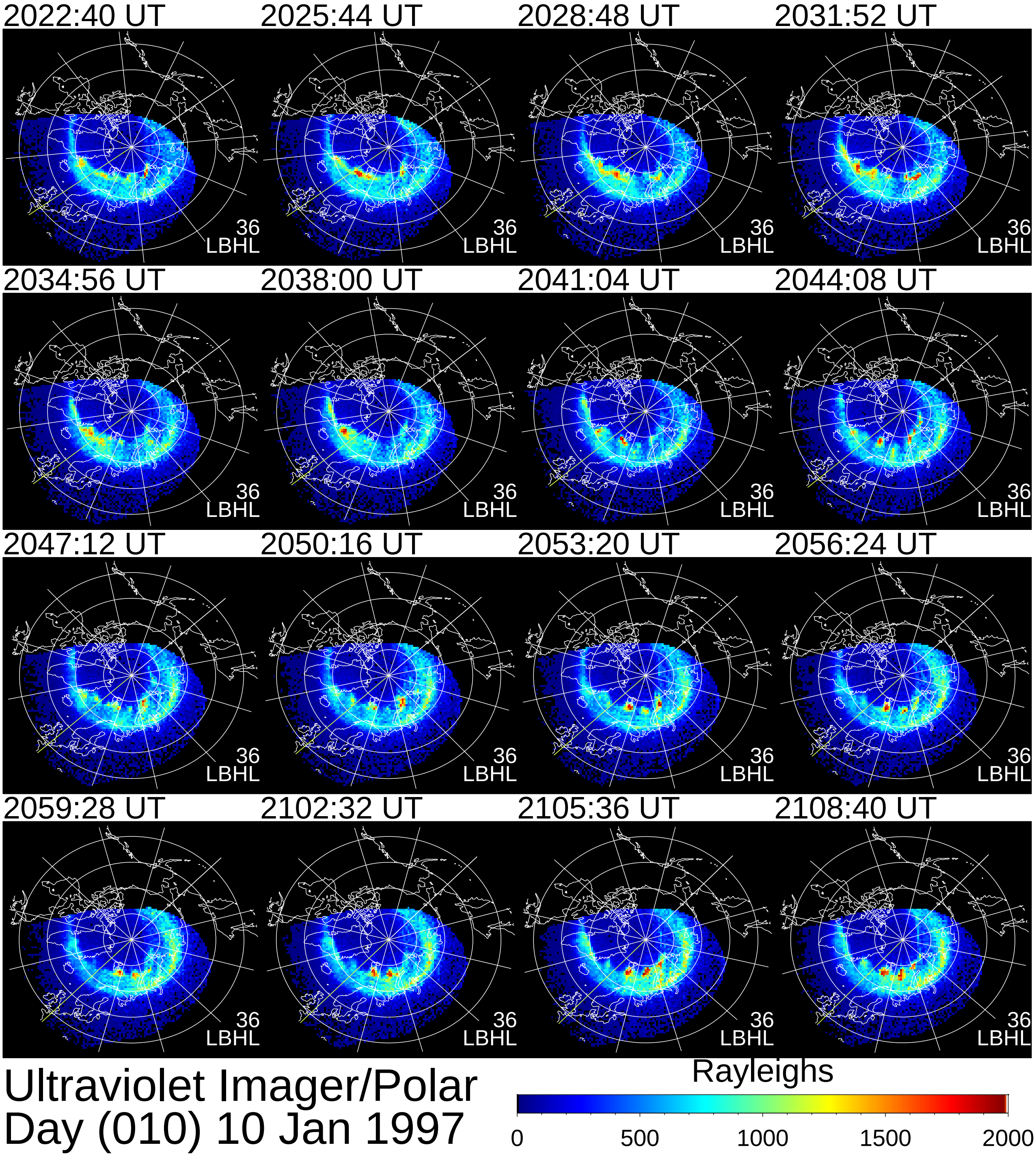
2022:40 UT
2025:44 UT
2028:48 UT
2031:52 UT
2034:56 UT
2038:00 UT
2041:04 UT
2044:08 UT
2047:12 UT
2050:16 UT
2053:20 UT
2056:24 UT
2059:28 UT
2102:32 UT
2105:36 UT
2108:40 UT
36
LBHL
Ultraviolet Imager/Polar
Day (010) 10 Jan 1997
Rayleighs
0
500
1000
1500
2000

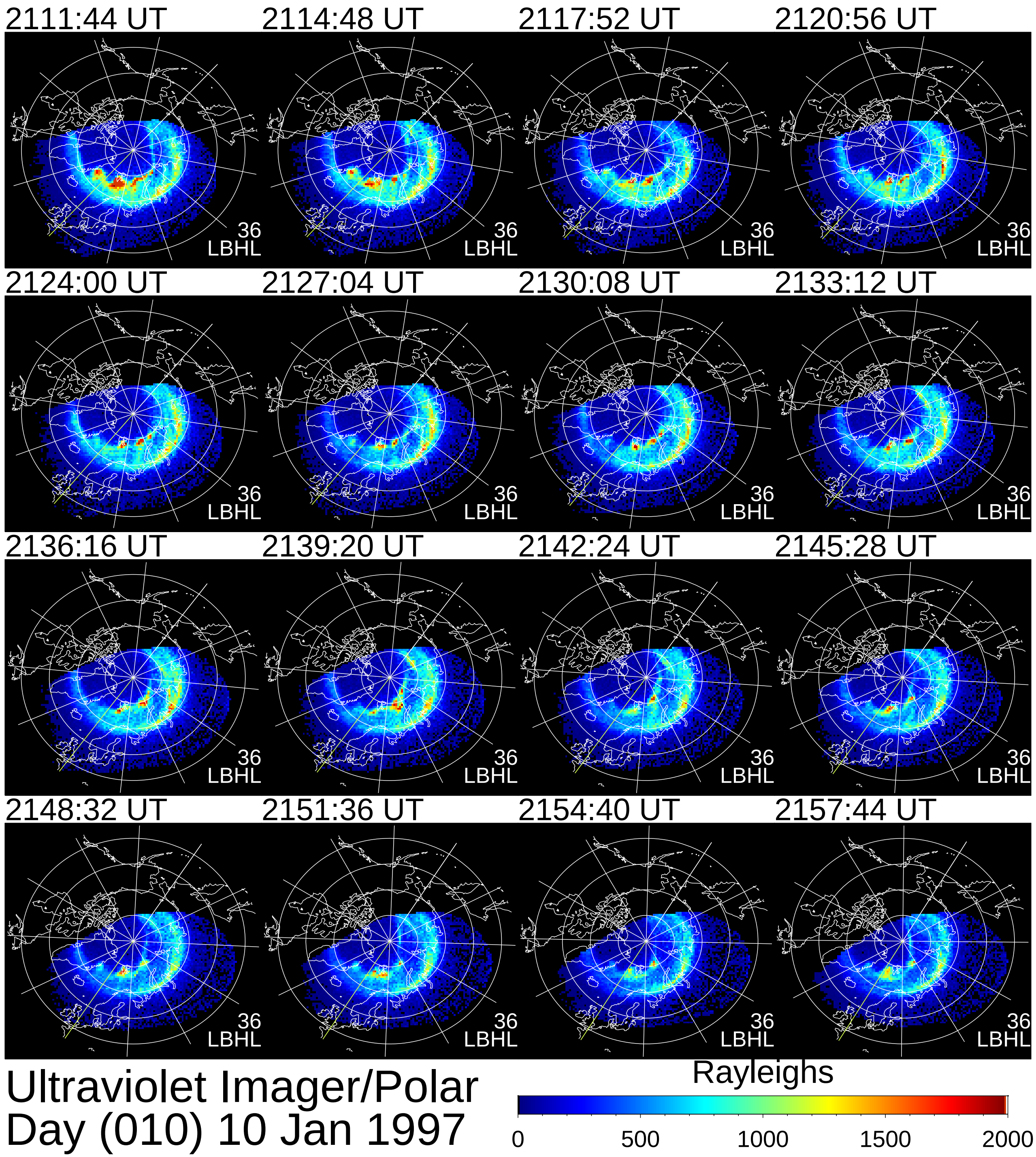
2111:44 UT
2114:48 UT
2117:52 UT
2120:56 UT
2124:00 UT
2127:04 UT
2130:08 UT
2133:12 UT
2136:16 UT
2139:20 UT
2142:24 UT
2145:28 UT
2148:32 UT
2151:36 UT
2154:40 UT
2157:44 UT
36
LBHL
Ultraviolet Imager/Polar
Day (010) 10 Jan 1997
Rayleighs
0
500
1000
1500
2000

Figure S3

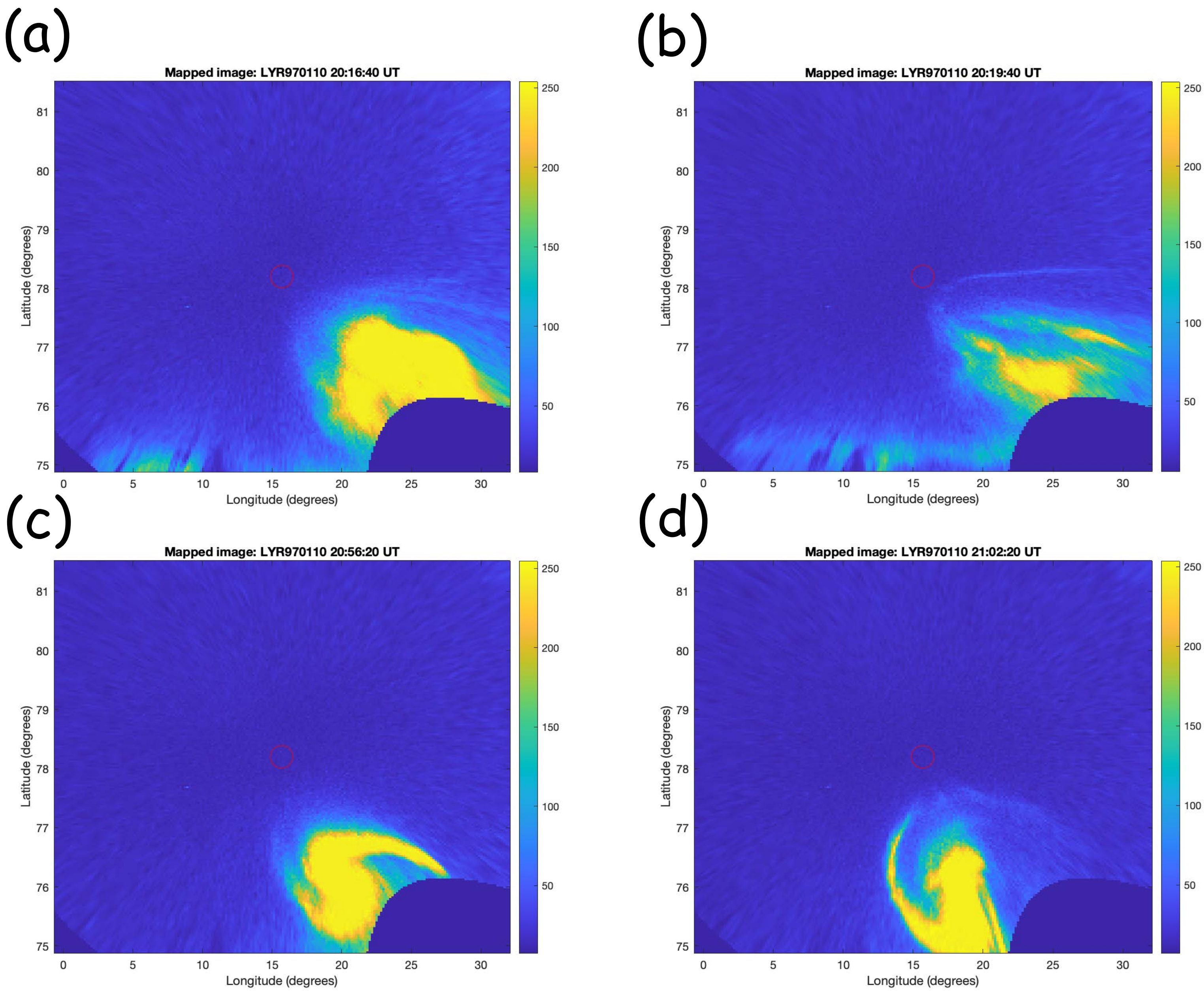
(a)
Mapped image: LYR970110 20:16:40 UT
(b)
Mapped image: LYR970110 20:19:40 UT
(c)
Mapped image: LYR970110 20:56:20 UT
(d)
Mapped image: LYR970110 21:02:20 UT
Latitude (degrees)
Longitude (degrees)
75
76
77
78
79
80
81
0
5
10
15
20
25
30
50
100
150
200
250

Figure S1. Time-series snapshots of Polar ultraviolet imager (UVI) of Lyman-Birge-Hopfield long (LBHL) emission with an integration time of 36.8 s in altitude adjusted corrected geomagnetic (AACGM) coordinates are shown for 3 h 16 min from 18:41:28 UT to 21:57:44 UT. The white circles are drawn every 10° from 60° to 80° magnetic latitude (MLat). Each panel is oriented such that the top, right, bottom and left sides correspond to noon (12h MLT (magnetic local time)), dawn (6h MLT), midnight (24h MLT), and dusk (18h MLT), respectively. The white lines are drawn every 2 h MLT. The color code is assigned according to the luminosity in units of Rayleigh.

Figure S2. Time-series of Polar UVI snapshots in geographic coordinates with coast lines for the same time interval as Figure S1 are shown in the same format as Figure S1.

Figure S3. The all-sky camera (ASC) data plots in geographic coordinates for four times are shown. Panels (a) – (d) show the plots for 20:16:40 UT, 20:19:40 UT, 20:56:20 UT, and 21:02:20 UT. The red circle in each panel indicates the location of the Longyearbyen station. In these plots, we assumed that the auroral emission height was 110 km. Vertical and horizontal axes give the geographical latitude and longitude in units of degree (°). The color code is assigned according to the auroral luminosity in units of Rayleigh.

Movie S1. Movie of consecutive images of the aurora spiral for 2 h from 20:00 UT to 22:00 UT on January 10, 1997, obtained from the all-sky camera (ASC) installed at Longyearbyen on Svalbard island is shown. The ASC covers a circular area with a diameter of about 600 km at an altitude of 110 km, with a field of view of 140°. Because the number of pixels corresponding to a 140° field of view is 440×440, the average spatial resolution of the image is about 1.4 km/pixel. The temporal resolution of the ASC's images is 20 s. The top, right, bottom, and left correspond to north, east, south, and west, respectively.

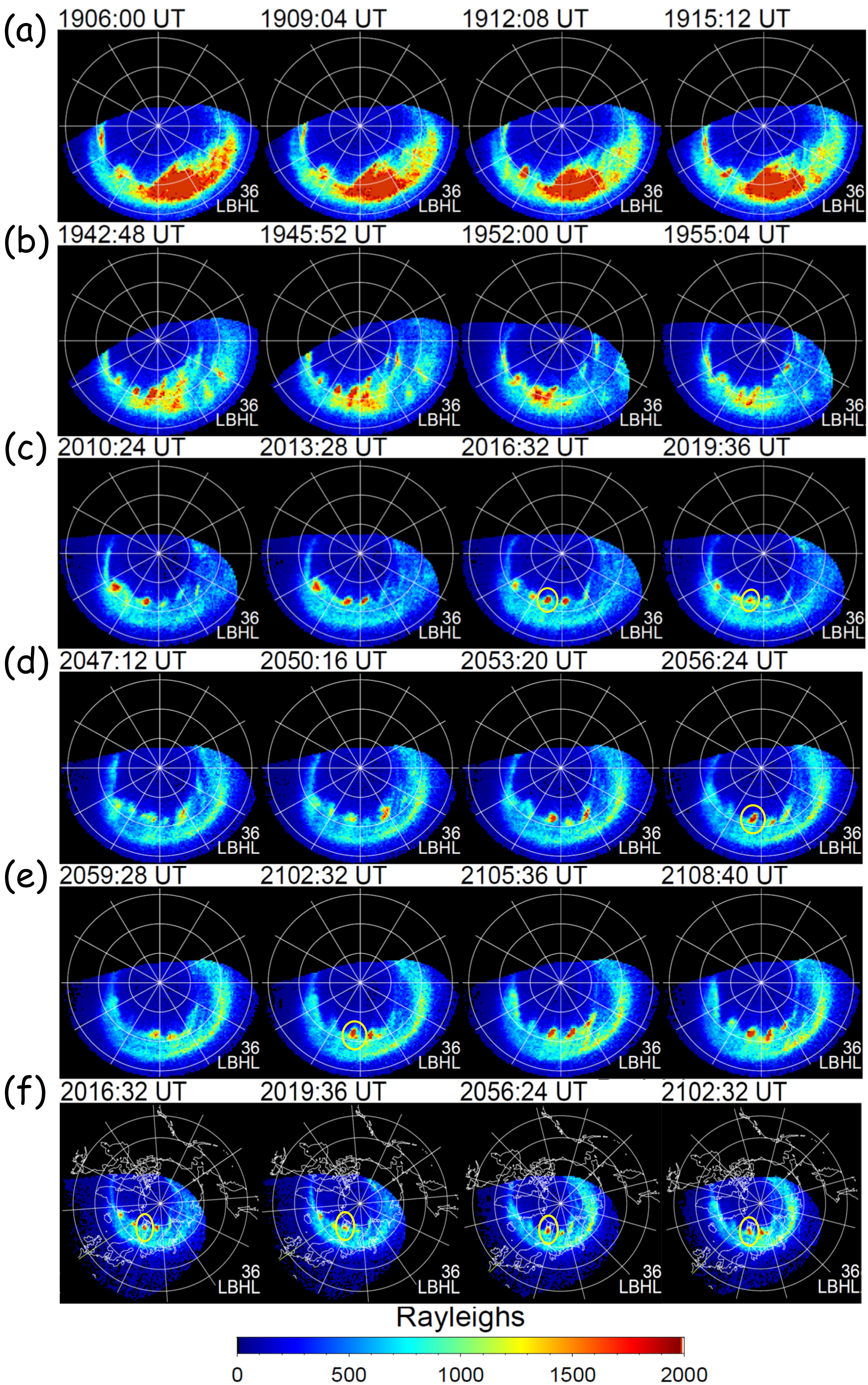

(a)
1906:00 UT
1909:04 UT
1912:08 UT
1915:12 UT
(b)
1942:48 UT
1945:52 UT
1952:00 UT
1955:04 UT
(c)
2010:24 UT
2013:28 UT
2016:32 UT
2019:36 UT
(d)
2047:12 UT
2050:16 UT
2053:20 UT
2056:24 UT
(e)
2059:28 UT
2102:32 UT
2105:36 UT
2108:40 UT
(f)
2016:32 UT
2019:36 UT
2056:24 UT
2102:32 UT
36
LBHL
Rayleighs
0
500
1000
1500
2000

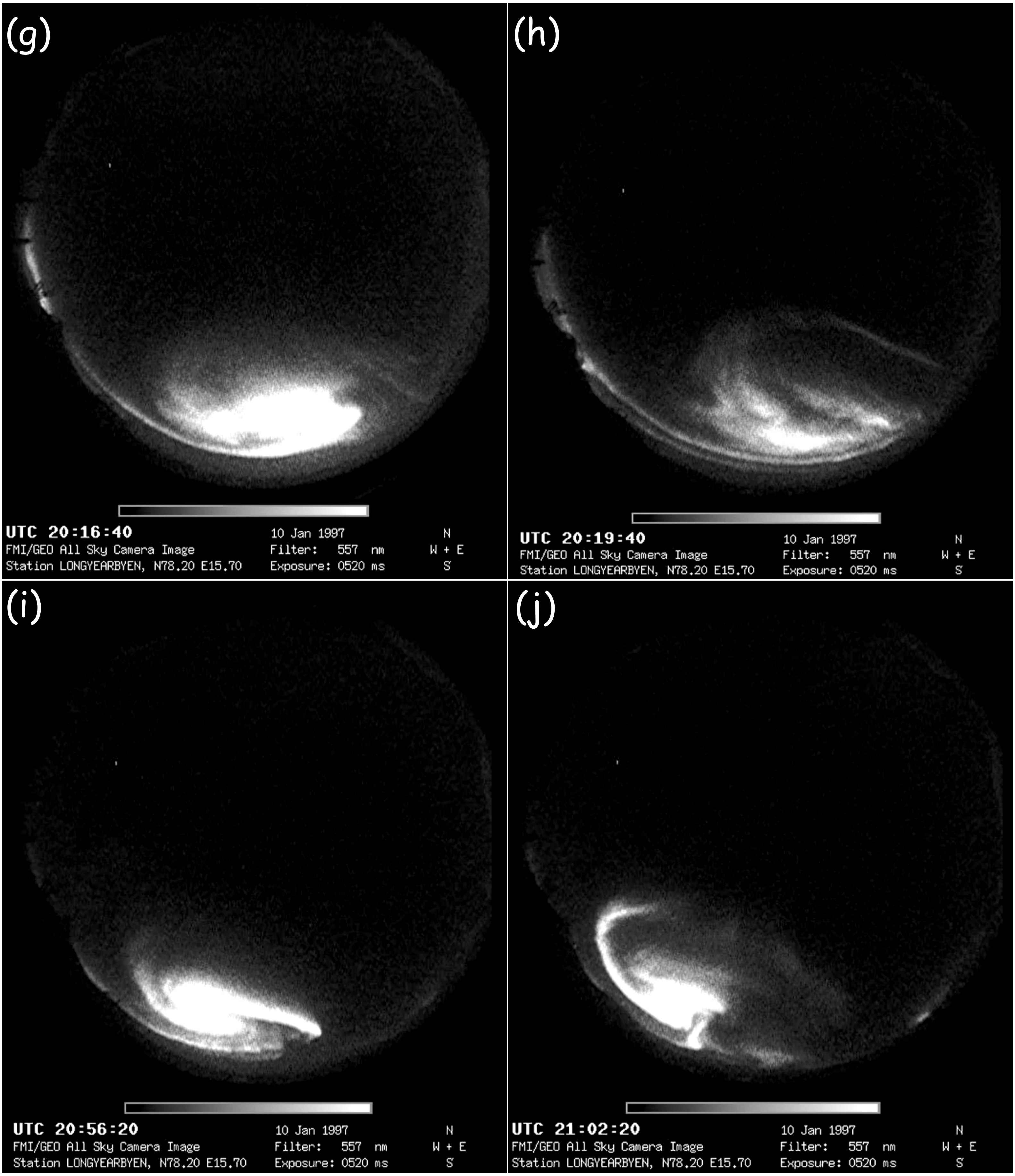

(g)
UTC 20:16:40
10 Jan 1997
FMI/GEO All Sky Camera Image
Filter: 557 nm
Station LONGYEARBYEN, N78.20 E15.70
Exposure: 0520 ms
N
W + E
S
(h)
UTC 20:19:40
10 Jan 1997
FMI/GEO All Sky Camera Image
Filter: 557 nm
Station LONGYEARBYEN, N78.20 E15.70
Exposure: 0520 ms
N
W + E
S
(i)
UTC 20:56:20
10 Jan 1997
FMI/GEO All Sky Camera Image
Filter: 557 nm
Station LONGYEARBYEN, N78.20 E15.70
Exposure: 0520 ms
N
W + E
S
(j)
UTC 21:02:20
10 Jan 1997
FMI/GEO All Sky Camera Image
Filter: 557 nm
Station LONGYEARBYEN, N78.20 E15.70
Exposure: 0520 ms
N
W + E
S